European Geosciences Union General Assembly 2024
Vienna, Austria, 14-19 April 2024
Session NP3.3:Climate Variability & Complex System Analysis Across Scales
EGU24-8588

Sharing is encouraged

Power-spectra of turbulent buoyant jets from laboratory measurements

K. Gkoutis, I. Papakonstantis, P. Dimitriadis and P. Papanicolaou

Department of Water Resources and Environmental Engineering
School of Civil Engineering
National Technical University of Athens

INTRODUCTION

- The investigation of turbulent jets is of great importance because jet flows arise in many engineering fields such as wastewater disposal and gaseous releases.
- 11 experiments of turbulent buoyant jets were carried out:
  6 with a temperature difference and
  5 experiments with salinity difference
- The experiments included flow visualization and concentration measurements using LIF technique.
- The results are compared to previous results from literature.

EXPERIMENTAL SET UP

- Main water Tank

  Dimensions: 1 x 0,8 x 0,7 m
- Secondary Tank- Heater with a capacity of 40 L for preparation of Rhodamine 6G solution
- Flow meter
- Measuring instruments (densitometers, digital measuring instrument YSI30, precision scales)
- Laser and rotating prism mirror
- Video camera
- Specially designed "curtains“ for darkened environment

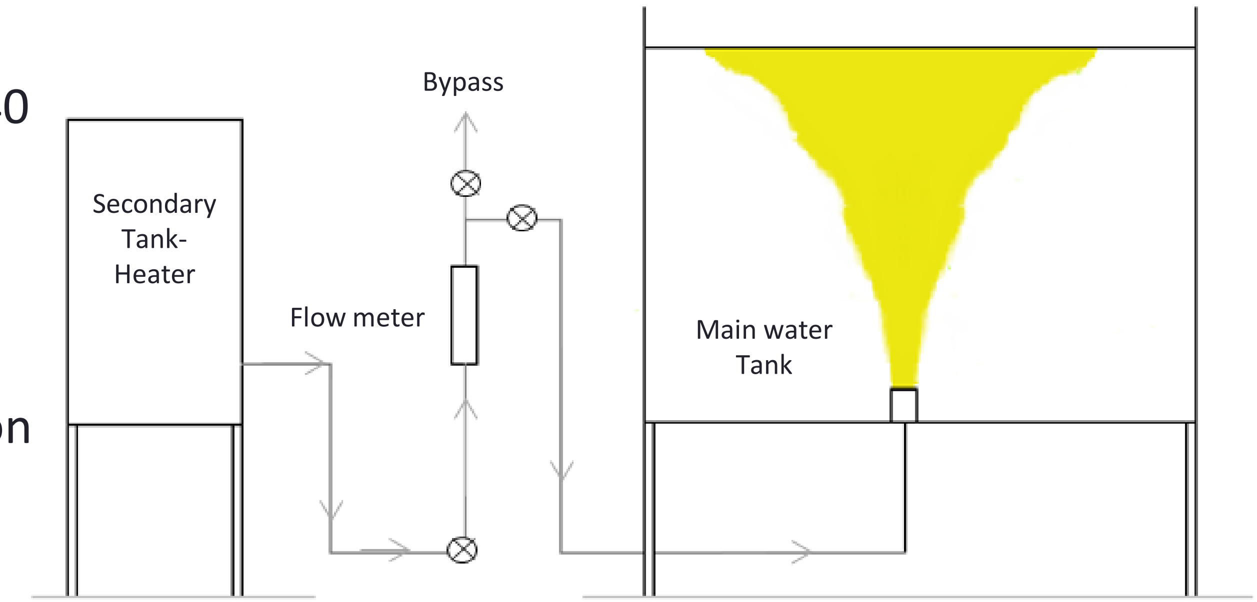

Figure 1.: Experimental set up

EXPERIMENTAL SET UP

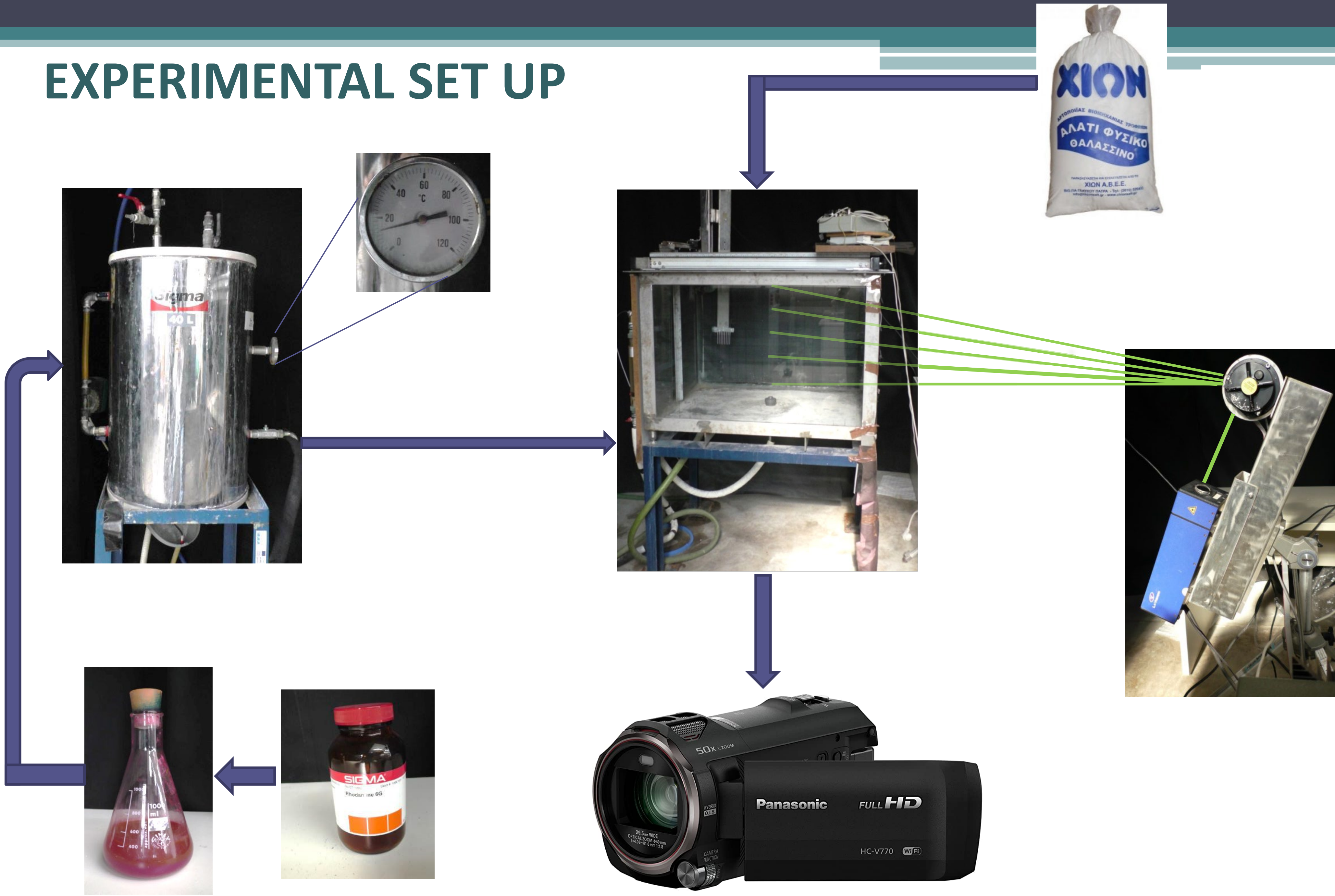

EXPERIMENTAL SET UP

- Main Water Tank 1 x 0,8 x 0,7 m
- Laser and rotating prism mirror
- Video camera

LIF TECHNIQUE (LASER INDUCED FLUORESCENCE)

Rhodamine 6G is added in the jet fluid. A laser sheet excites the dye and the fluorescent light emitted is recorded by means of a video camera.

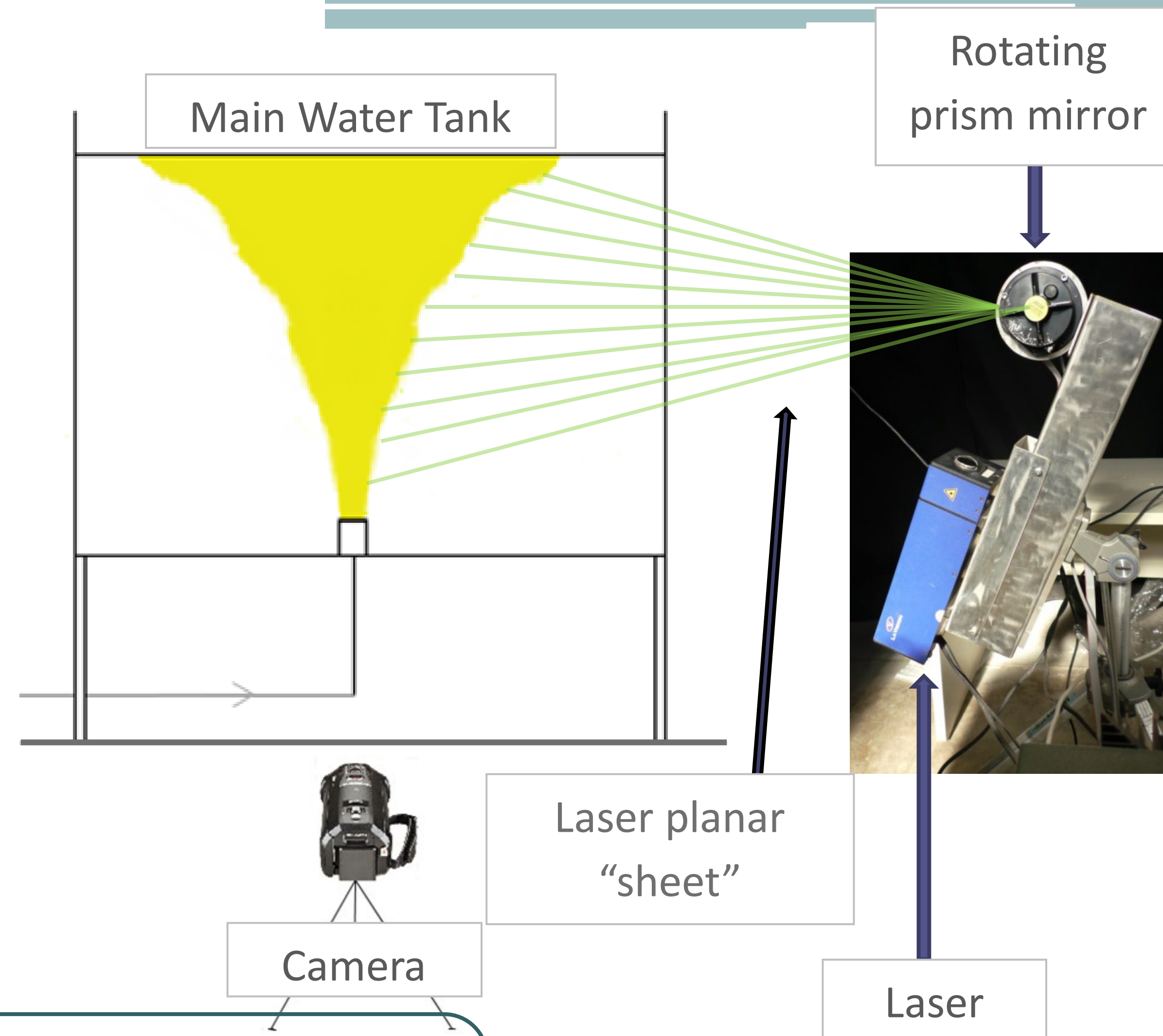

Flow visualization and high accuracy concentration measurements by correlating light intensity and concentration

INITIAL EXPERIMENTAL CONDITIONS

- 11 experiments with LIF technique
- 6 experiments with temperature difference

  (ΔT between 23°C - 31 °C) ⟶ (Δρ between 0,6% and 0,82%)
- 5 experiments with salinity difference

  (Δs betweem 25,2 ppt and 26,2 ppt) ⟶ (Δρ between 1,8% and 1,9%)
- Outlet diameter 1,5 cm
- Flow rate between 14,75 cm^3/s and 27,15 cm^3/s
- Densimetric Froude number F_o between 1,72 and 3,73
- Reynolds number Re at the outlet between 1222 and 3136

CHARACTERISTIC IMAGES

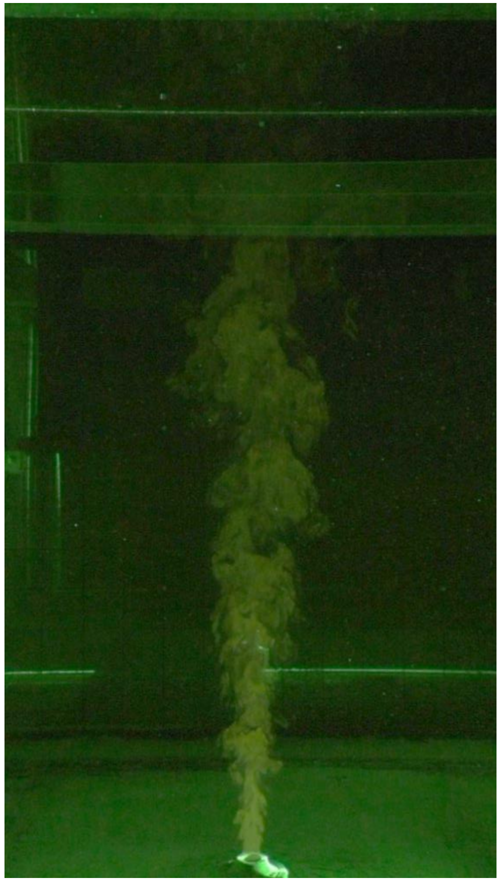

t=90 s

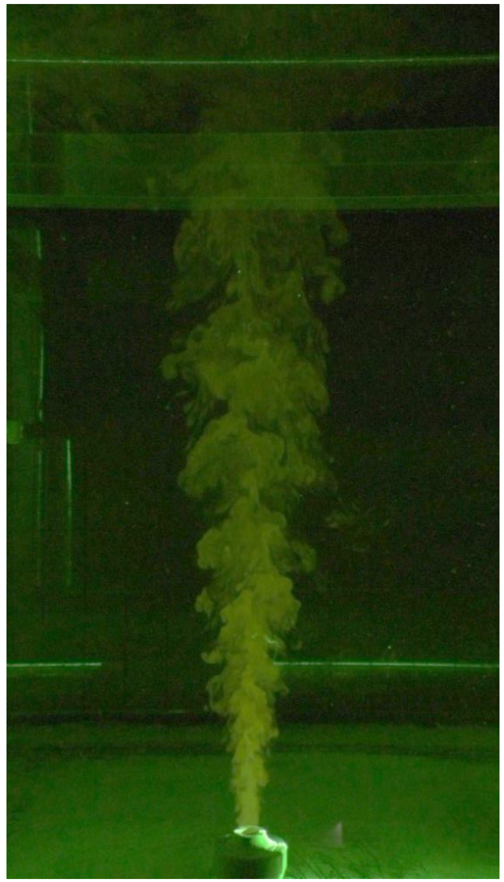

t=90 s

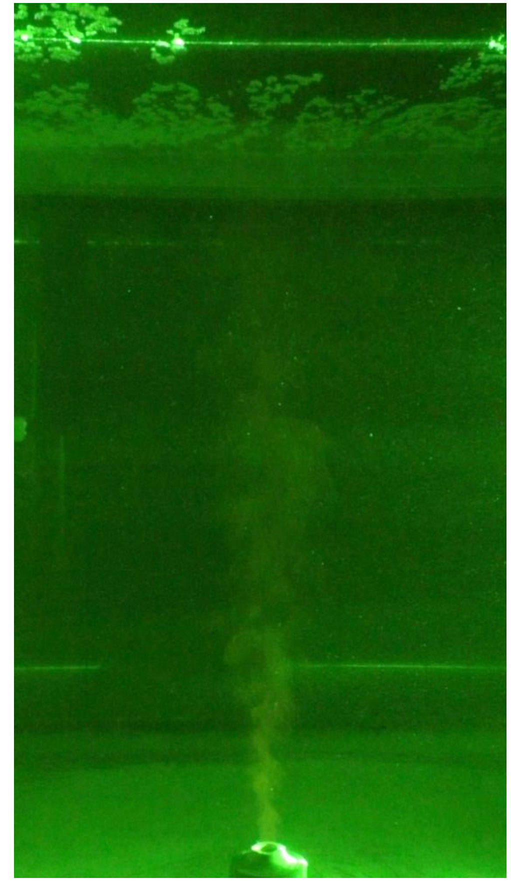

t=90 s

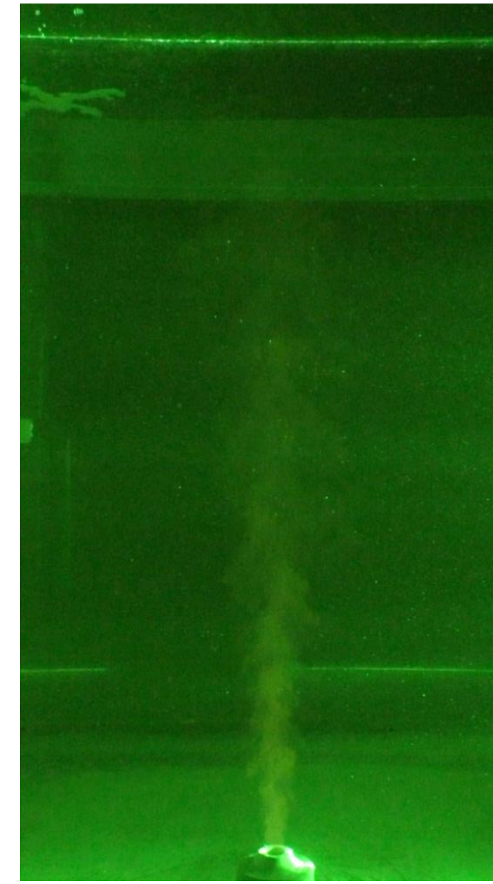

t=90 s

MEAN AND RMS CONCENTRATION- TURBULENCE INTENSITY

- For each concentration C_i :

$$c_i = \bar{c} + c_i'$$

where $\bar{C}$ is the mean of the values και c_i' is the turbulent fluctuation of concentration

- The mean concentration is :

$$\bar{c} = \frac{\sum_{i=1}^{i=N} c_i}{N} = c$$

Processing: Removal of mean concentration c_α and transformation in dimensionless form using C_M (Maximum value)

- The RMS concentration is: $\sqrt{\overline{c'^2}} = \mathrm{C_{RMS}} = \sqrt{\frac{\sum_{i=1}^{i=N}(c_i - \bar{c})^2}{N}}$

Processing: transformation in dimensionless form with C_M (Maximum mean concentration)

- N=3000-4000 (frames)

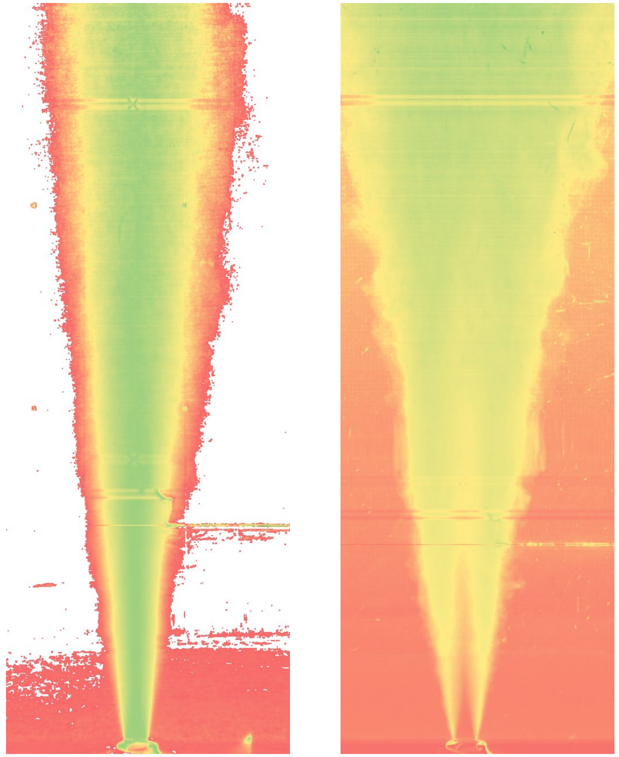

Figure 2.: Mean and RMS concentration after processing (Experiment Exp.9T)

MEAN CONCENTRATION DISTRIBUTIONS

- The distributions satisfactorily approximate the dimensionless Gaussian distribution, indicating self-similarity
- Decrease in values on the right side due to light attenuation
- Calculation of attenuation:

$$P'' = P' e^{-(\eta_w + \varepsilon_0 C(x))\Delta x}$$

where η_w is the attenuation in water (cm^{-1}), ε_0 is the attenuation coefficient due to the existence of Rhodamine 6G (cm-1)(μg l^{-1})-1 and C(x) continuous concentration function of σε μg/l^{-1} ,P´ the power of the beam entering the length element Δx and P´´the power exiting from it.

↓

Symmetric diagram

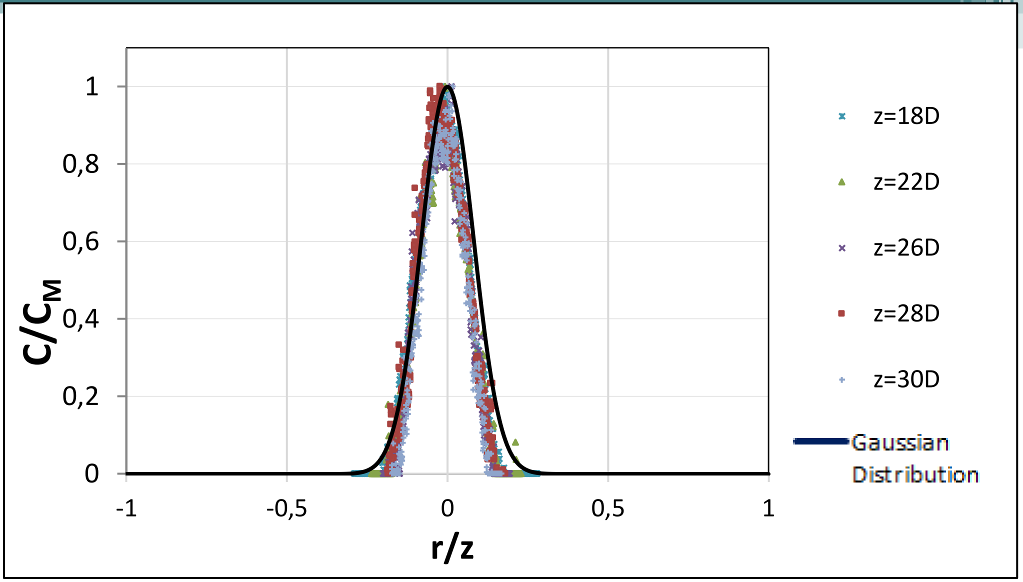

Figure 3.: Transverse distribution of the mean concentration at various distances from the outflow for Experiment Exp.6T

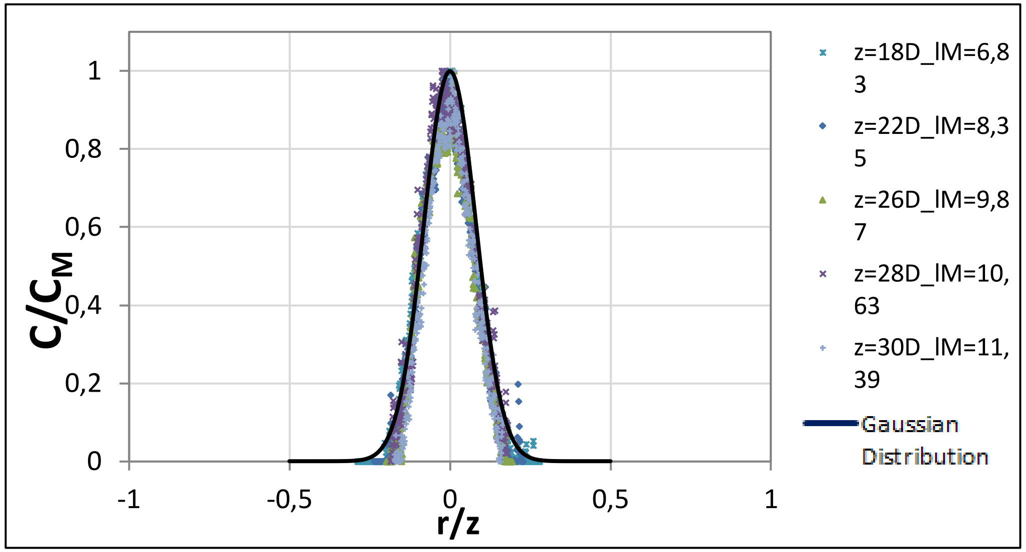

Figure 4.: Transverse distribution of the mean concentration at various distances from the outflow for Experiment Exp.6T after attenuation calculation

RESULTS – TRANSVERSE DISTRIBUTIONS OF THE MEAN CONCENTRATION

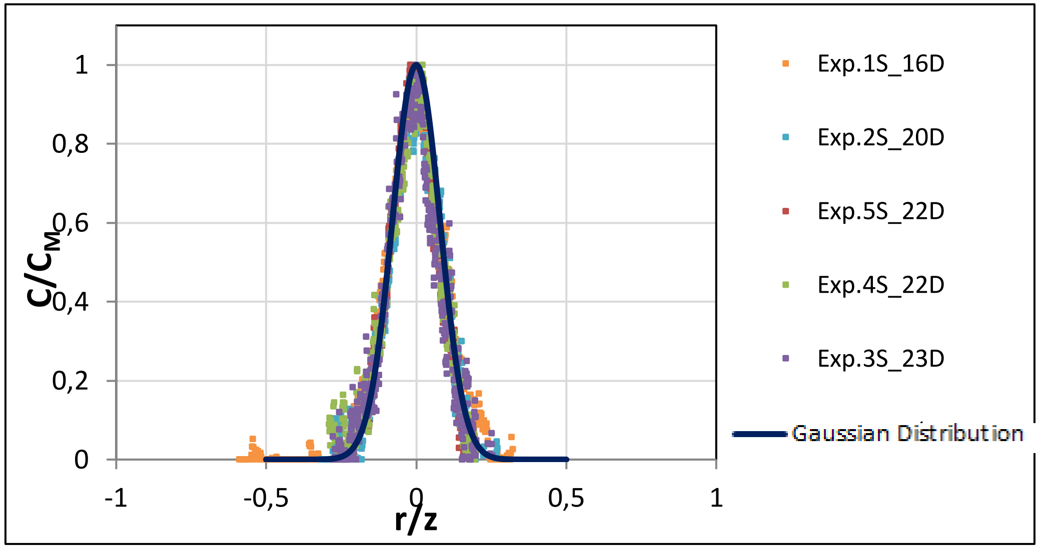

Figure 5.:Transverse distribution of the mean concentration at various vertical distances from the outflow for experiments with salinity difference.

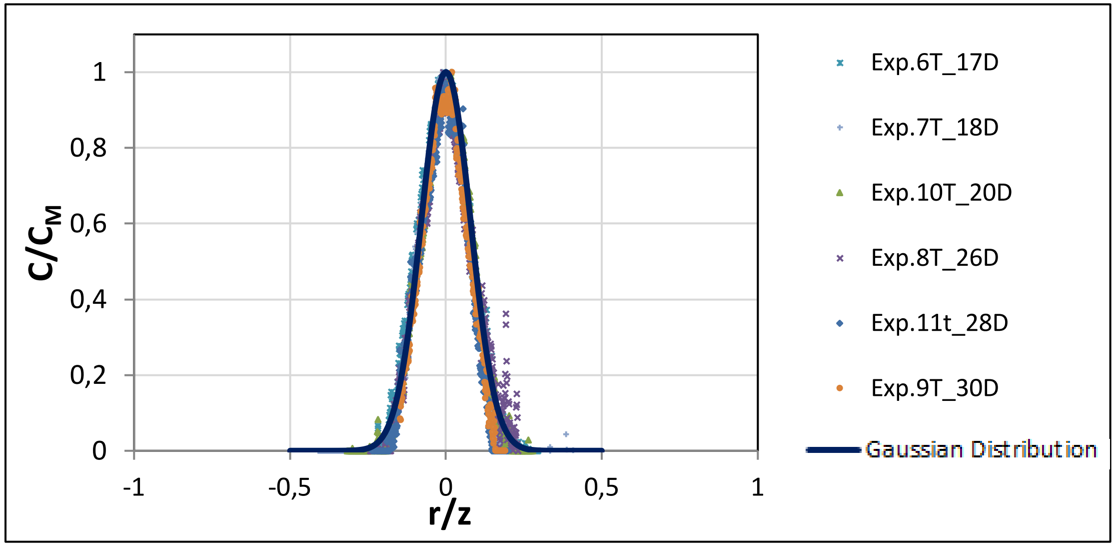

Figure 6.:Transverse distribution of the mean concentration at various vertical distances from the outflow for experiments with temperature difference.

- The distributions satisfactorily approximate the dimensionless Gaussian distribution:

$$C\,/\,C_M = e^{-r^2/bc^2}$$

  where b_c is the width of the concentration distribution
- Self-similarity

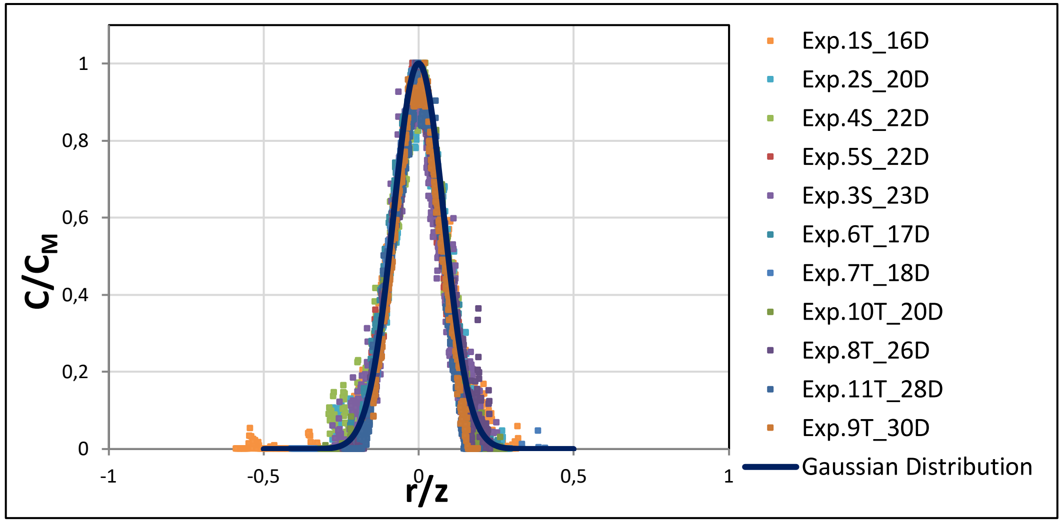

Figure 7.: Transverse distribution of the mean concentration at various vertical distances from the outflow for the entire set of experiments

POWER SPECTRUM

The estimated PS of the concentration are presented below. The Power Spectrum (E(k)) is calculated using Fast Fourier Transformation given by:

$$\mathrm{E}(k) = \lim_{T\to\infty} \frac{|C(k)|^2}{T} \qquad C(f) = \int_{-\infty}^{+\infty} c(t) \cdot e^{-2\pi i f t}\, dt$$

where is t the time vector (sec), T the total duration of the time-series (sec) and f the frequency (Hz)

The log-slope of the power spectral estimates from all experiments approximate the Kolmogorov slope of -5/3, in agreement with theoretical results for the inertial subrange.

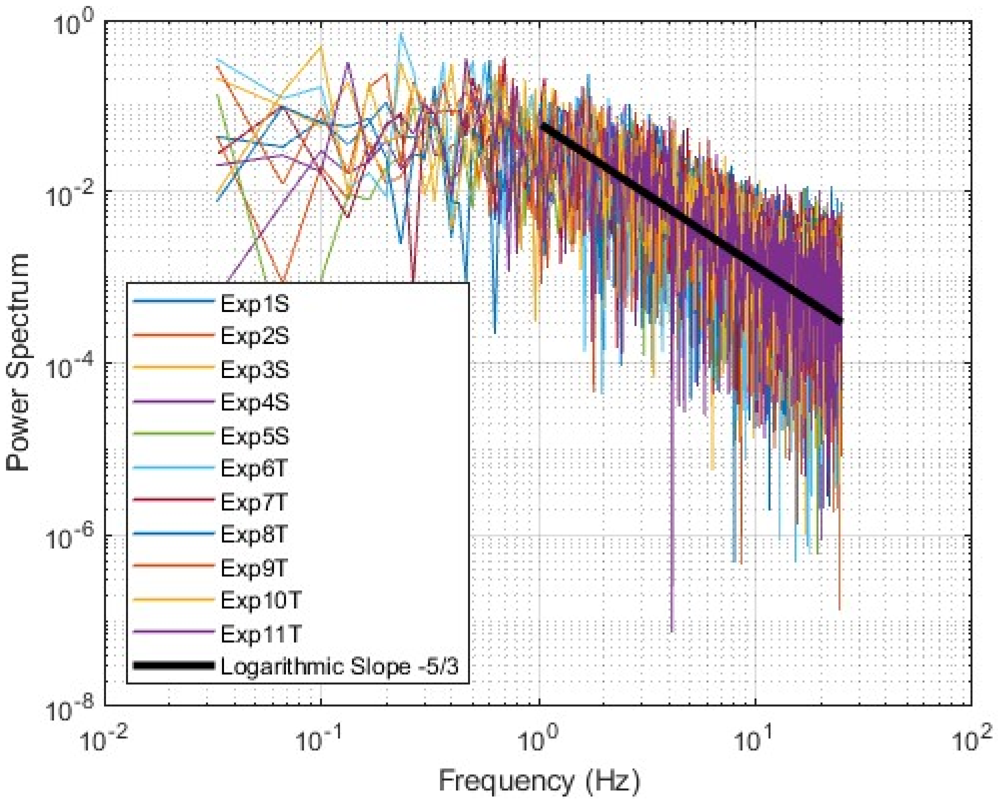

Figure 8. : Power spectral estimates for the entire set of experiments at the buoyant jet centerline at dimensionless distance z=5,84 l_M

CONCLUSION

- The LIF method achieves flow visualization and concentration measurement with high precision, without interfering with the flow
- The distributions of the dimensionless mean concentration C/C_M with respect to the dimensionless distance r/z from the axis of the buoyant jet satisfactorily approximate the Gaussian dimensionless distribution
- The log slope of the power spectral estimates satisfactorily approximate Kolmogorov model slope of -5/3

GRAPHS

Exp.1S

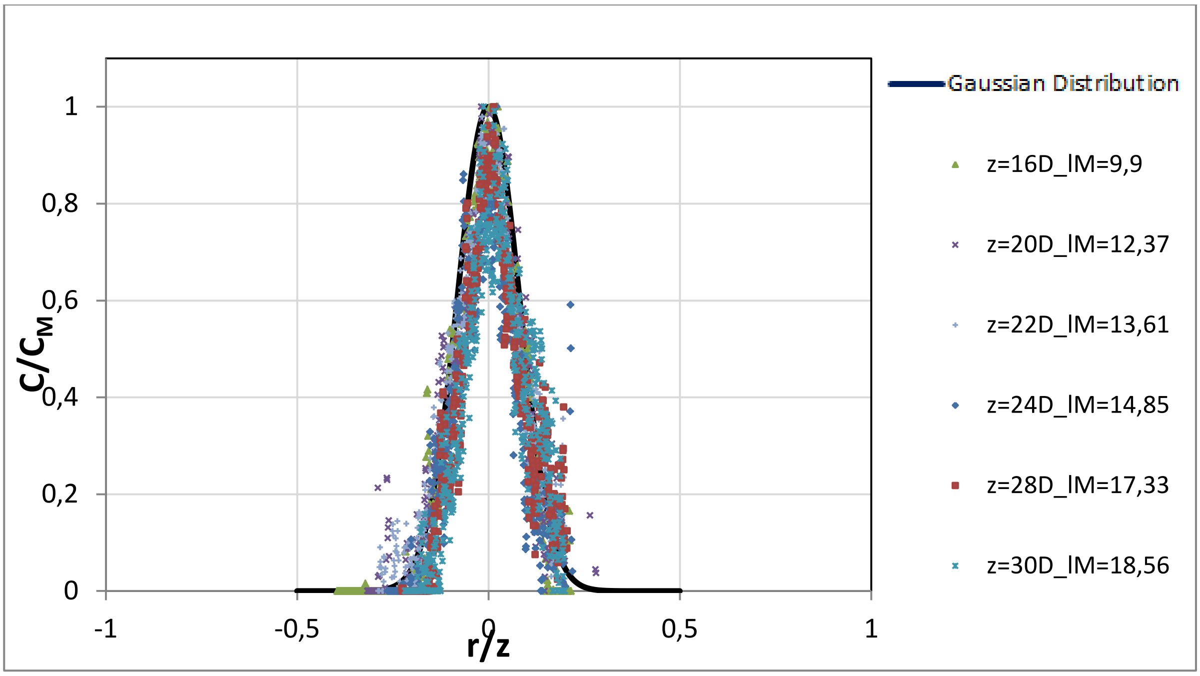

Figure A.1 Transverse distribution of the mean concentration at various vertical distances from the outflow from experiment Exp.1S

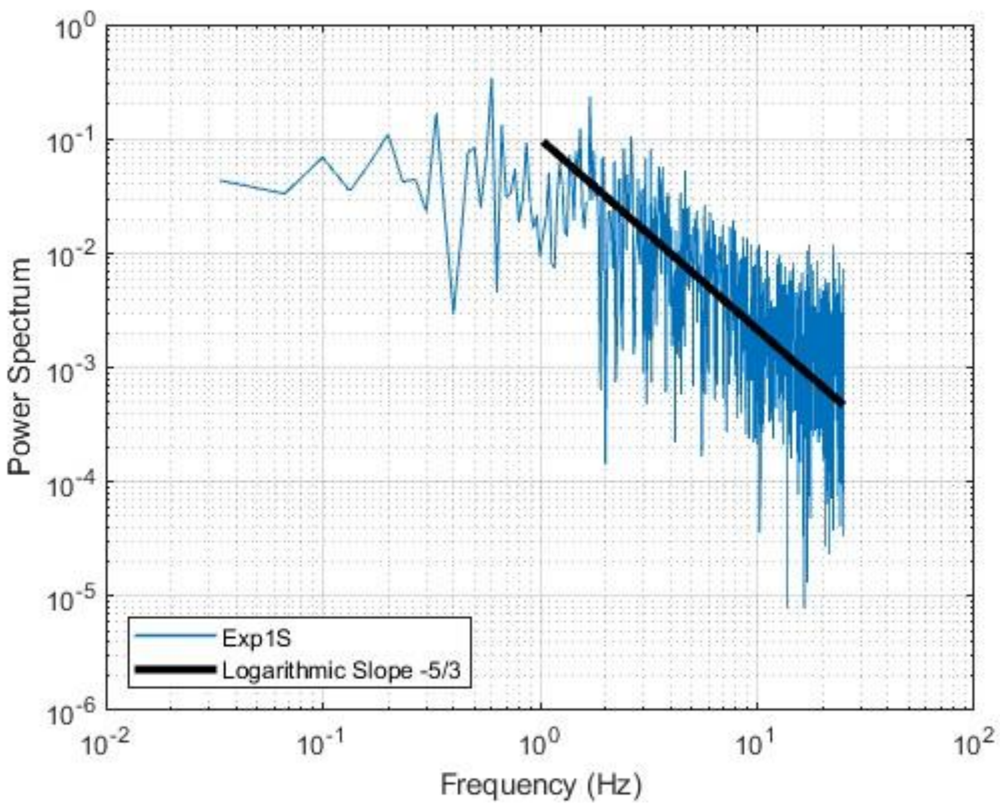

Figure A.2 Power spectral estimate at the buoyant jet centerline at dimensionless distance z=5,84 l_M for experiment Exp.1S

Exp.2S

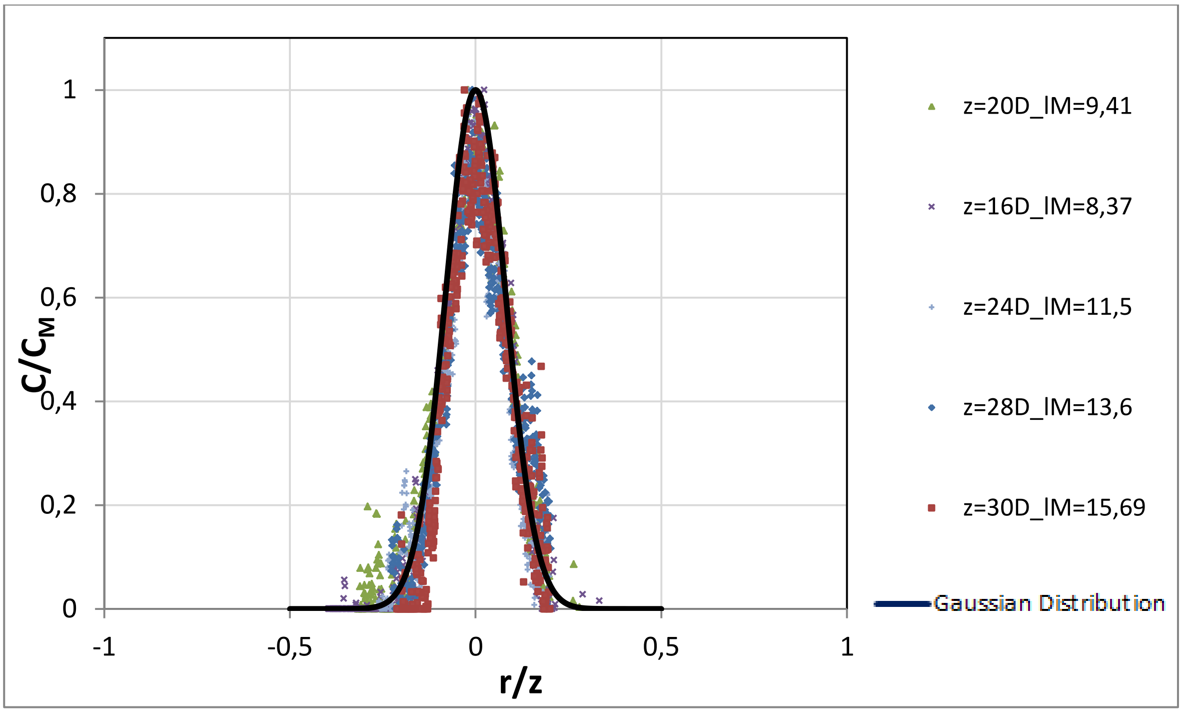

Figure A.3 Transverse distribution of the mean concentration at various vertical distances from the outflow from experiment Exp.2S

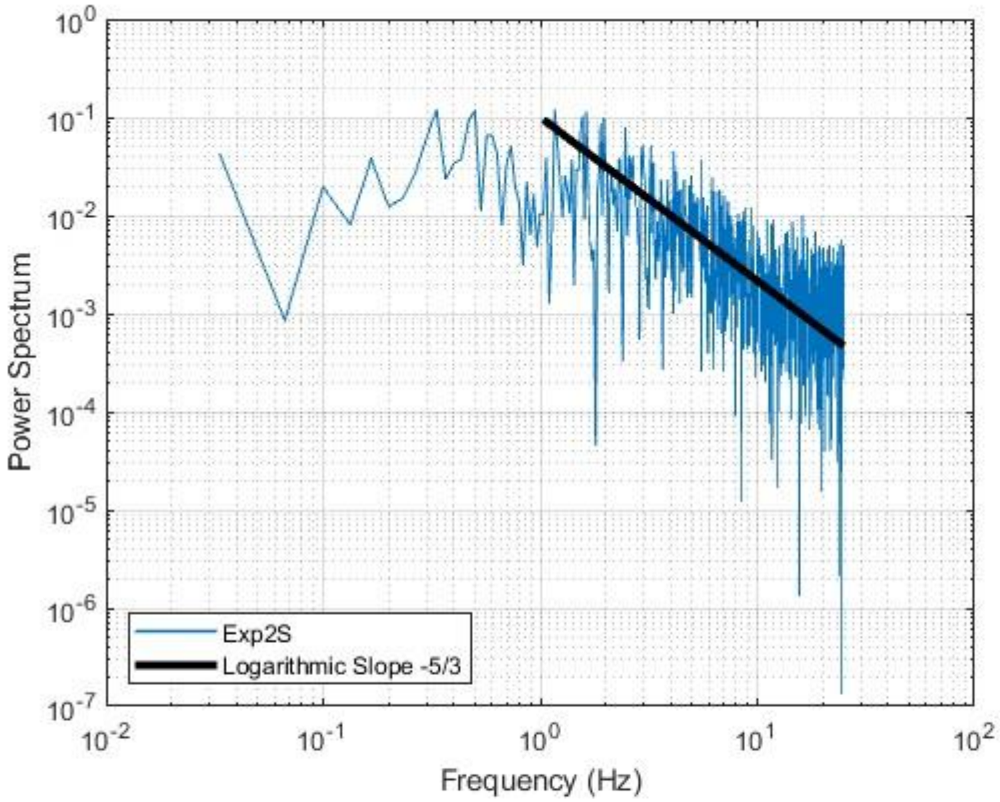

Figure A.4 Power spectral estimate at the buoyant jet centerline at dimensionless distance z=5,84 l_M for experiment Exp.2S

Exp.3S

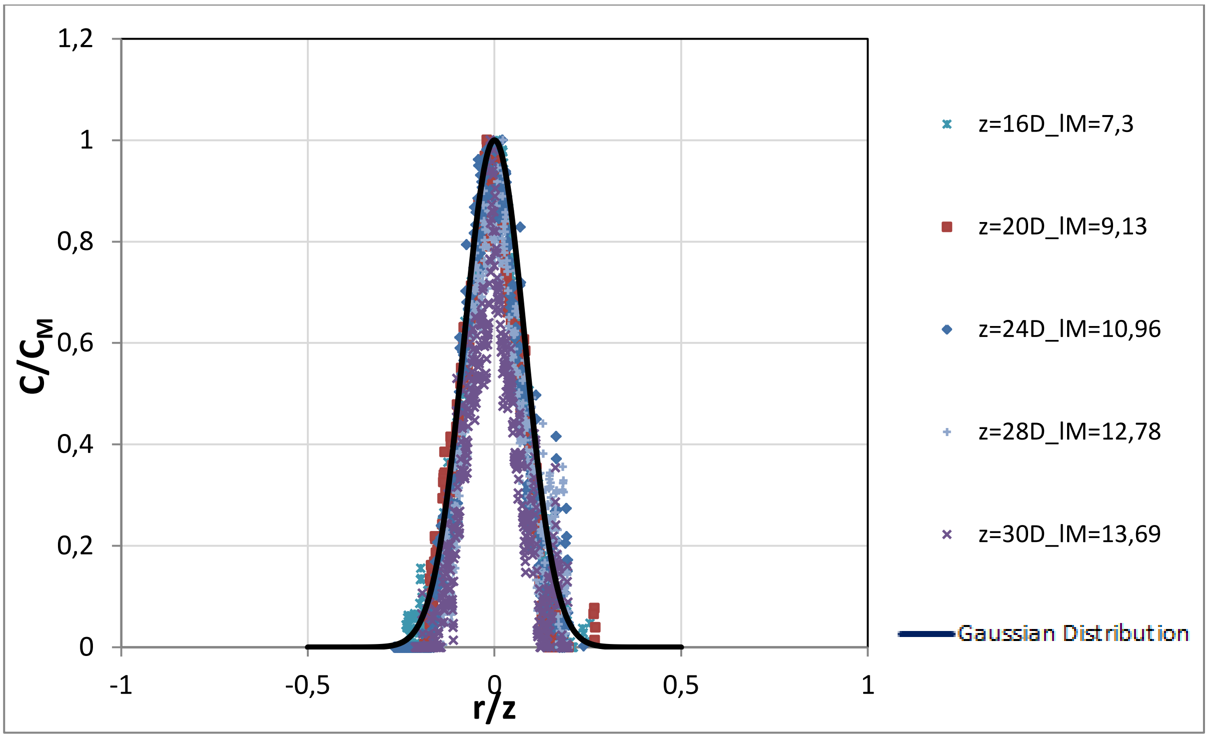

Figure A.5 Transverse distribution of the mean concentration at various vertical distances from the outflow from experiment Exp.3S

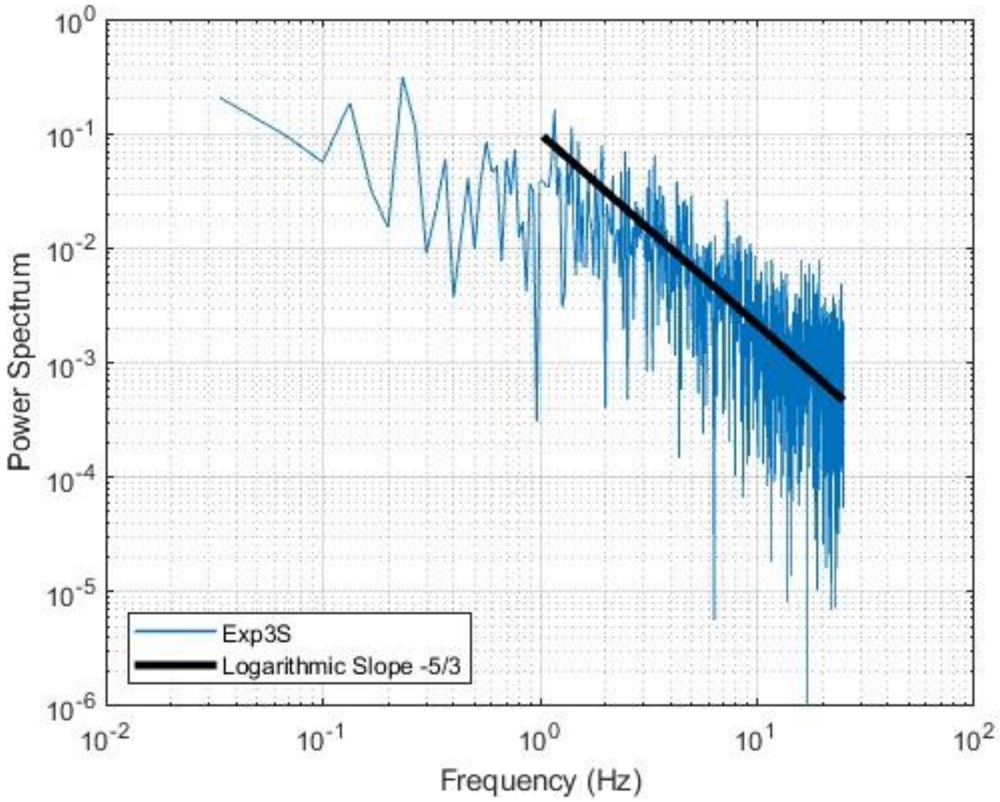

Figure A.6 Power spectral estimate at the buoyant jet centerline at dimensionless distance z=5,84 l_M for experiment Exp.3S

Exp.4S

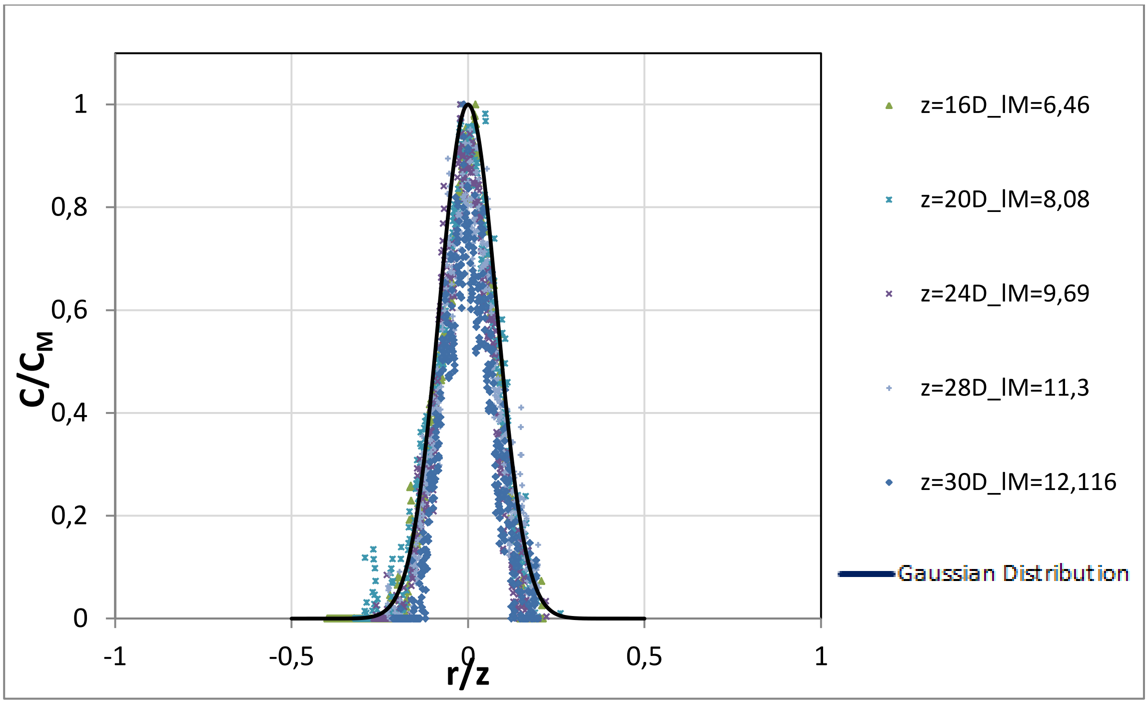

Figure A.7 Transverse distribution of the mean concentration at various vertical distances from the outflow from experiment Exp.4S

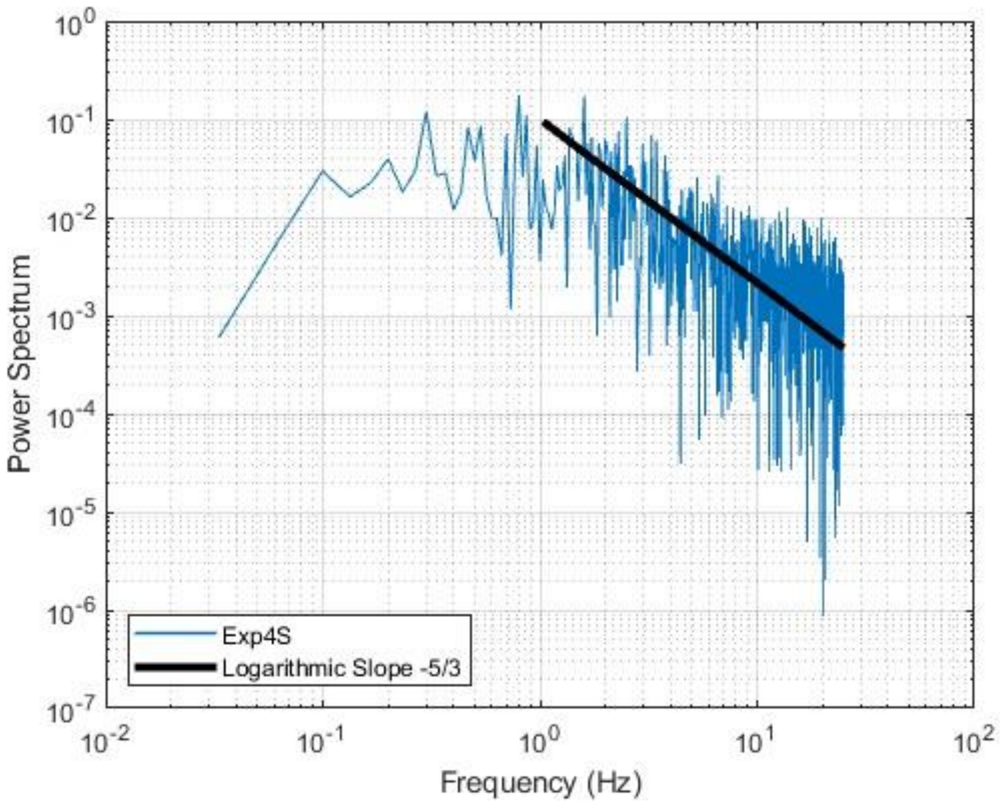

Figure A.8 Power spectral estimate at the buoyant jet centerline at dimensionless distance z=5,84 l_M for experiment Exp.3S

Exp.5S

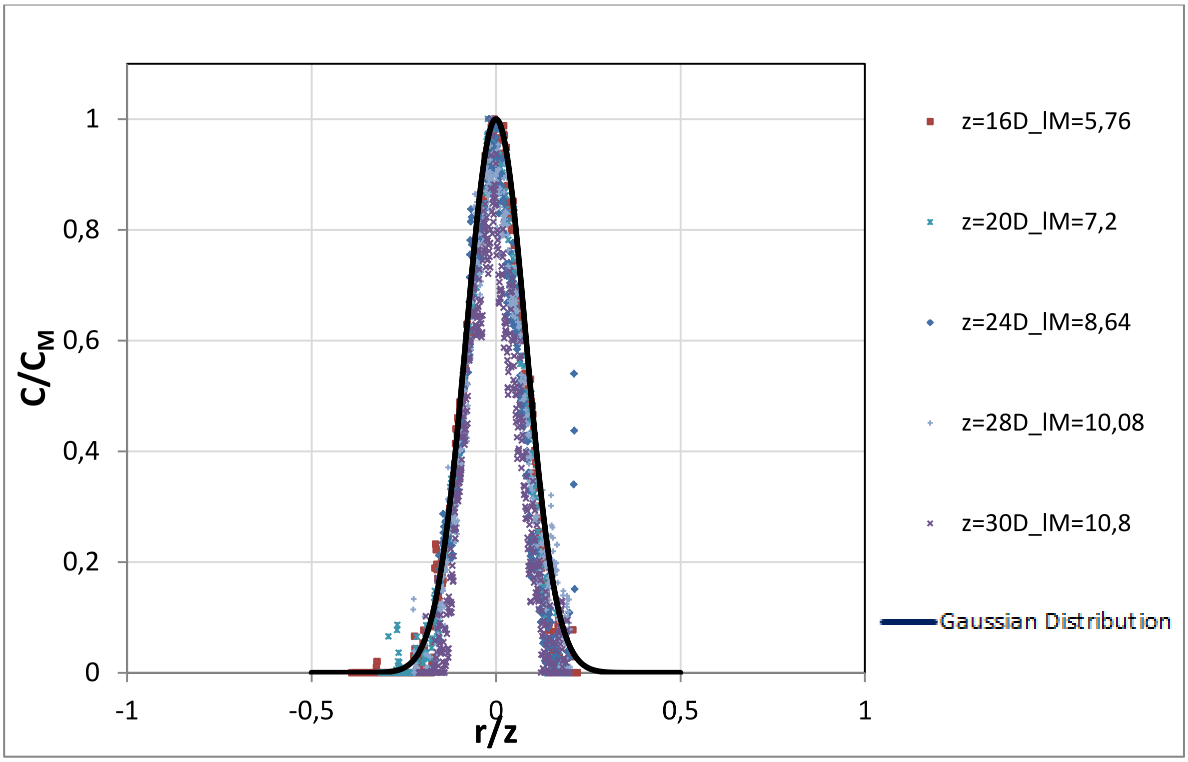

Figure A.9 Transverse distribution of the mean concentration at various vertical distances from the outflow from experiment Exp.5S

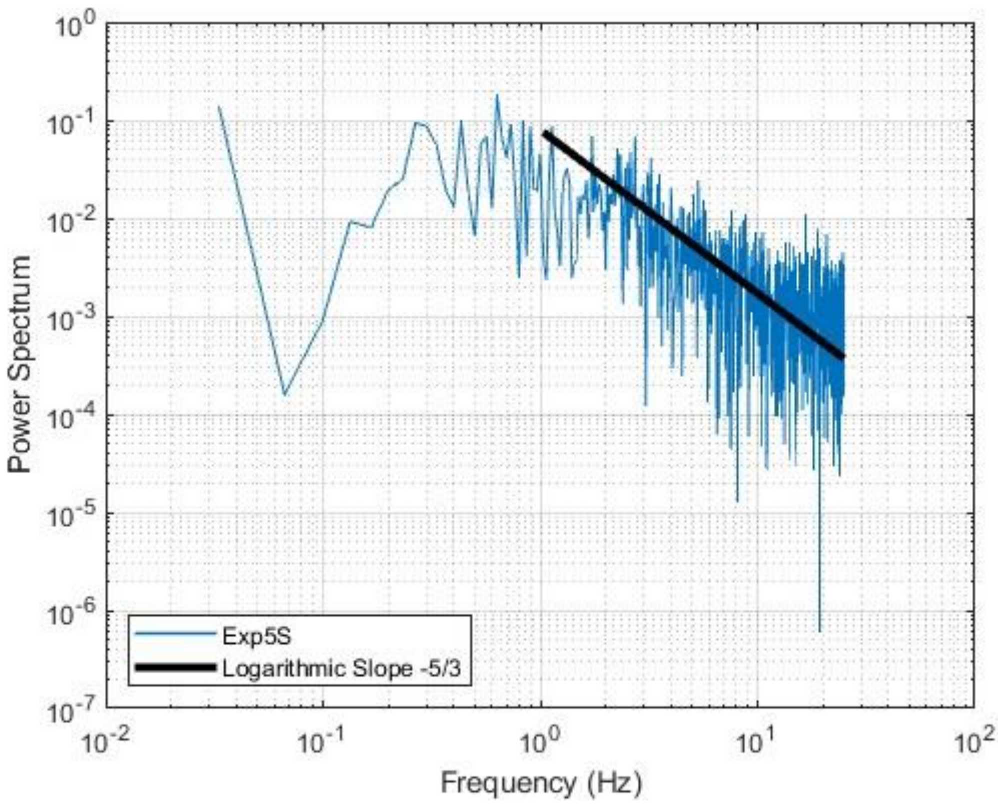

Figure A.10 Power spectral estimate at the buoyant jet centerline at dimensionless distance z=5,84 l_M for experiment Exp.5S

Exp.6T

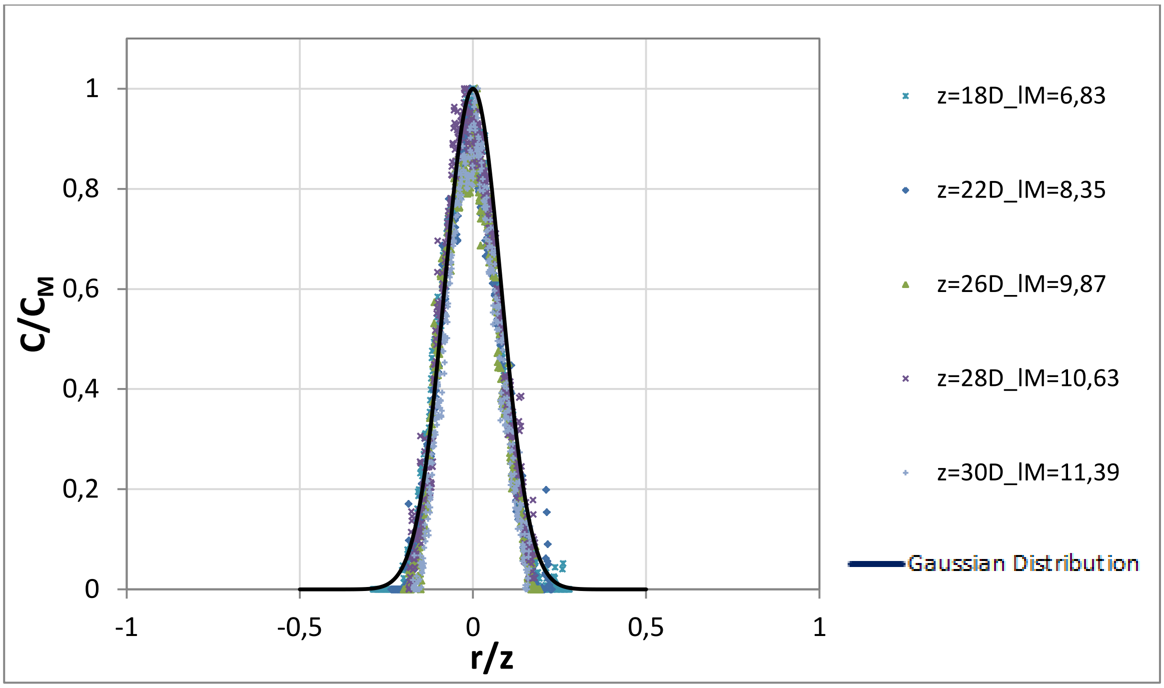

Figure A.11 Transverse distribution of the mean concentration at various vertical distances from the outflow from experiment Exp.6T

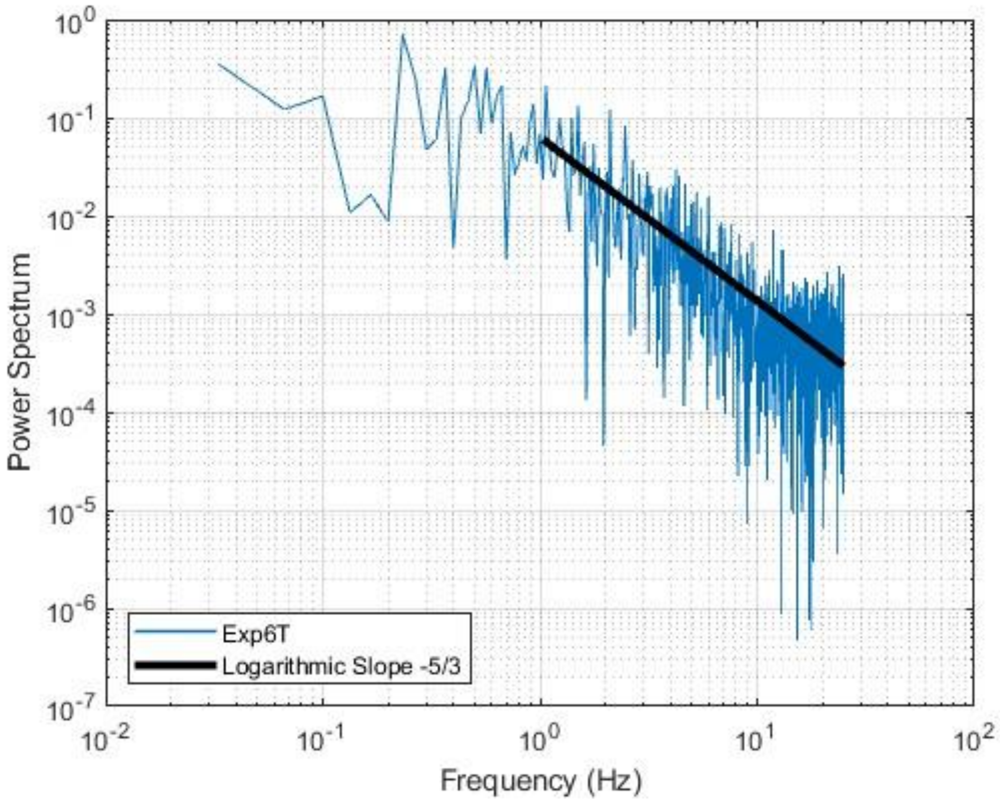

Figure A.12 Power spectral estimate at the buoyant jet centerline at dimensionless distance z=5,84 l_M for experiment Exp.6T

Exp.7T

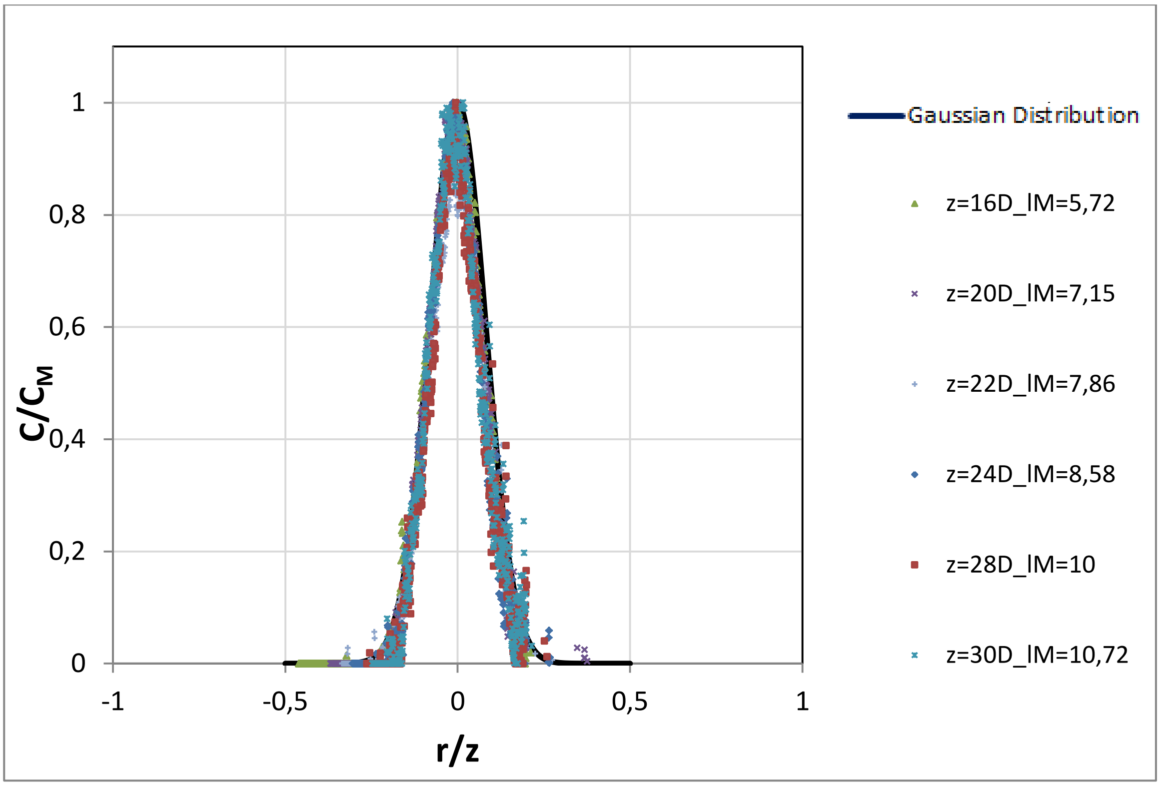

Figure A.13 Transverse distribution of the mean concentration at various vertical distances from the outflow from experiment Exp.7T

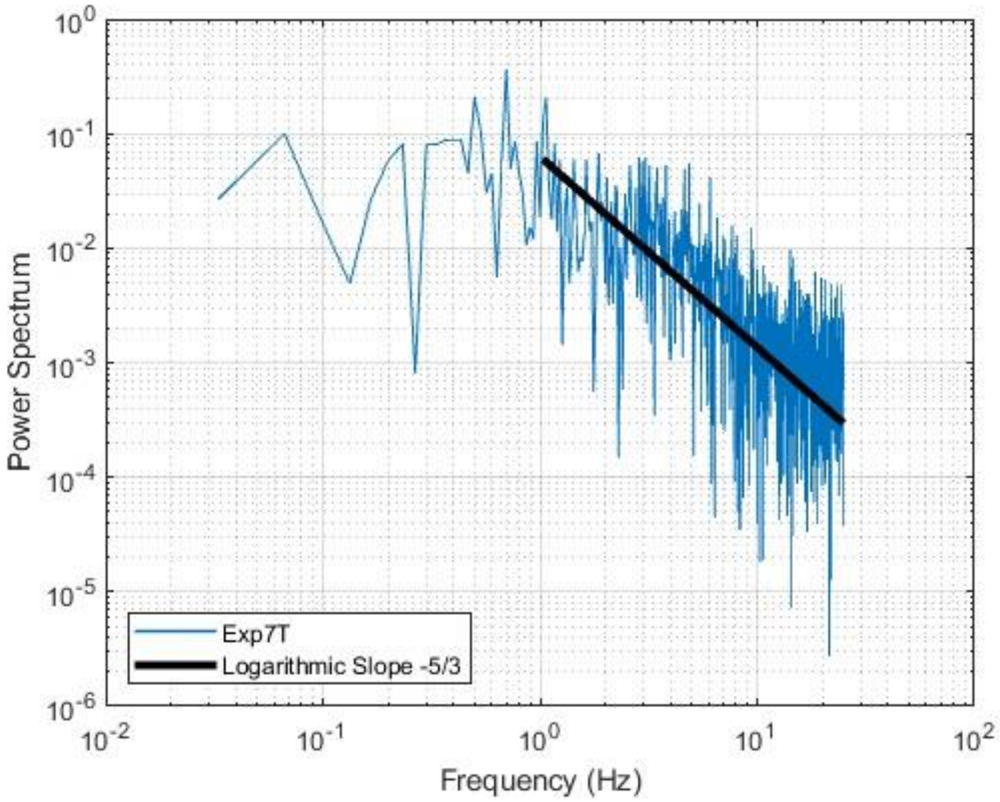

Figure A.14 Power spectral estimate at the buoyant jet centerline at dimensionless distance z=5,84 l_M for experiment Exp.7T

Exp.8T

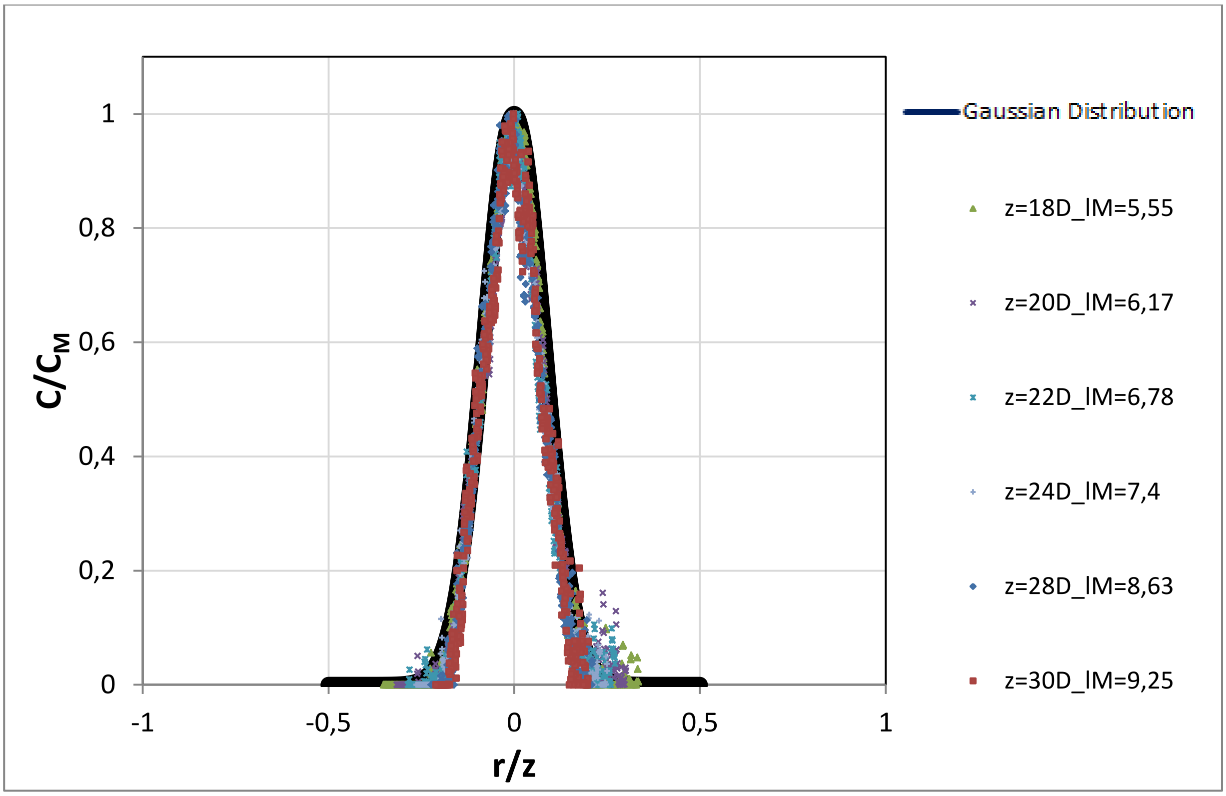

Figure A.15 Transverse distribution of the mean concentration at various vertical distances from the outflow from experiment Exp.8T

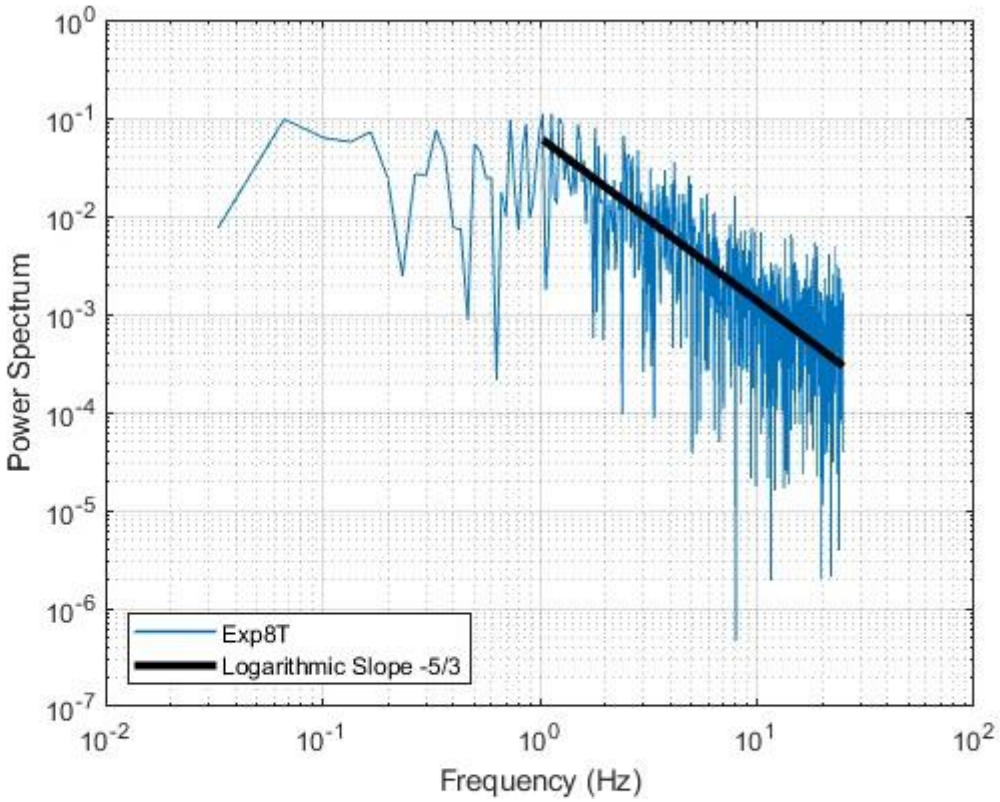

Figure A.16 Power spectral estimate at the buoyant jet centerline at dimensionless distance z=5,84 l_M for experiment Exp.8T

Exp.9T

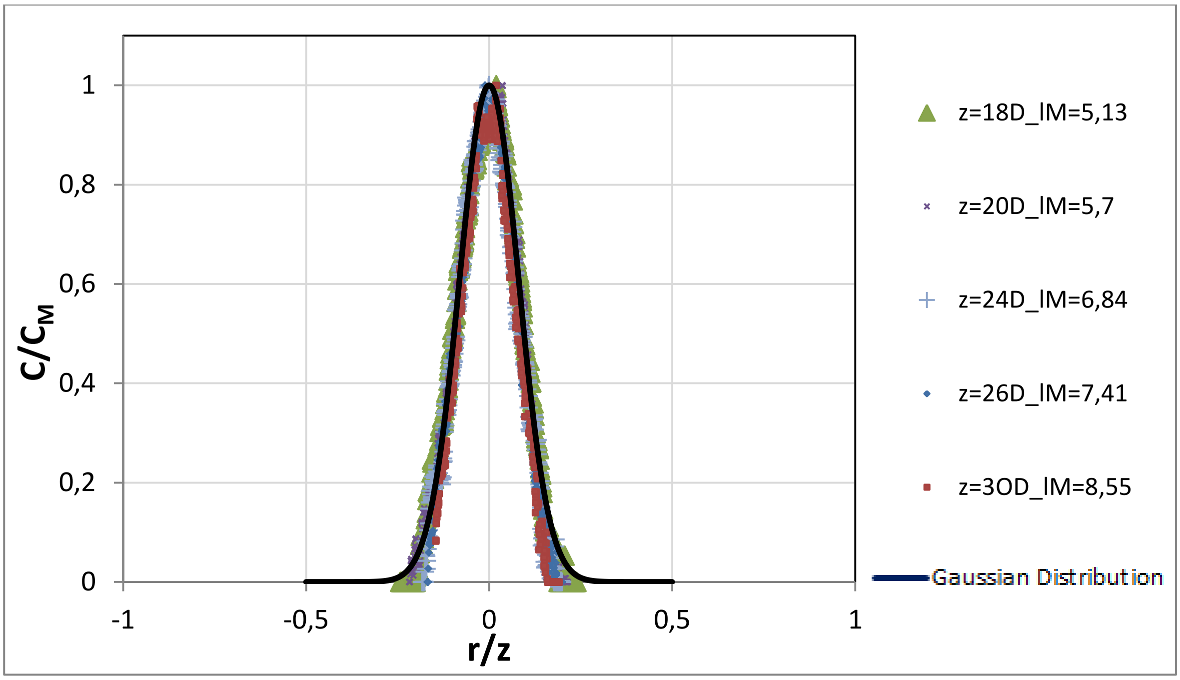

Figure A.17 Transverse distribution of the mean concentration at various vertical distances from the outflow from experiment Exp.9T

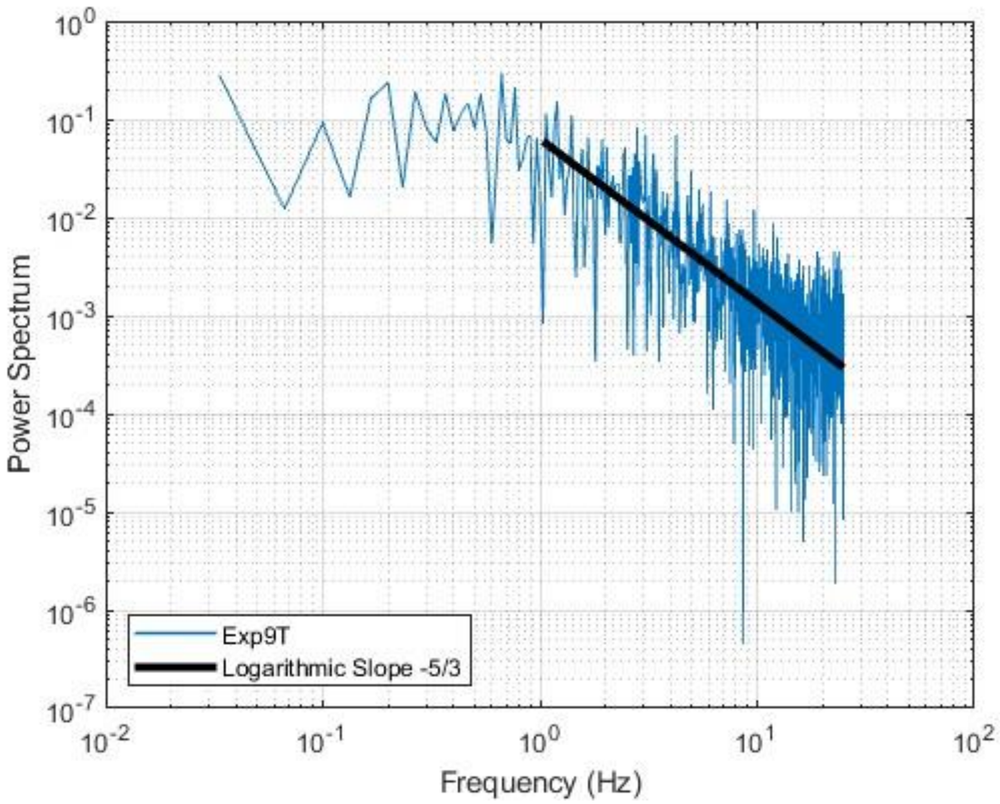

Figure A.18 Power spectral estimate at the buoyant jet centerline at dimensionless distance z=5,84 l_M for experiment Exp.9T

Exp.10T

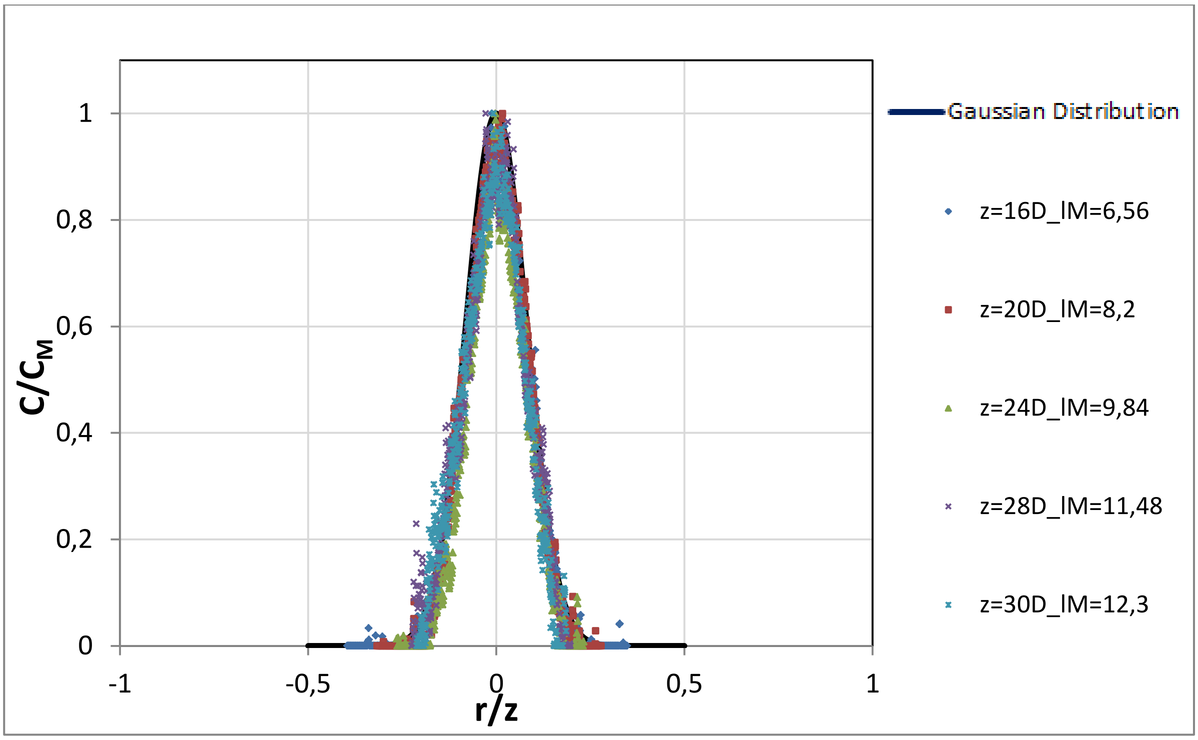

Σχήμα A.19 Transverse distribution of the mean concentration at various vertical distances from the outflow from experiment Exp.10T

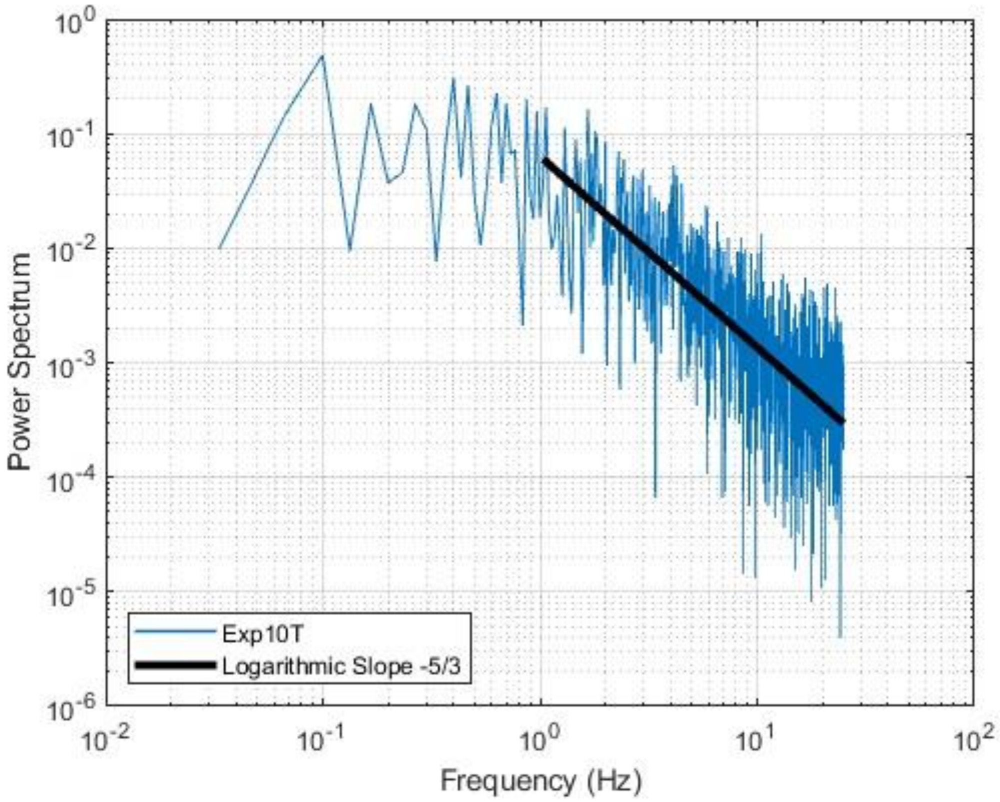

Figure A.20 Power spectral estimate at the buoyant jet centerline at dimensionless distance z=5,84 l_M for experiment Exp.10T

Exp.11T

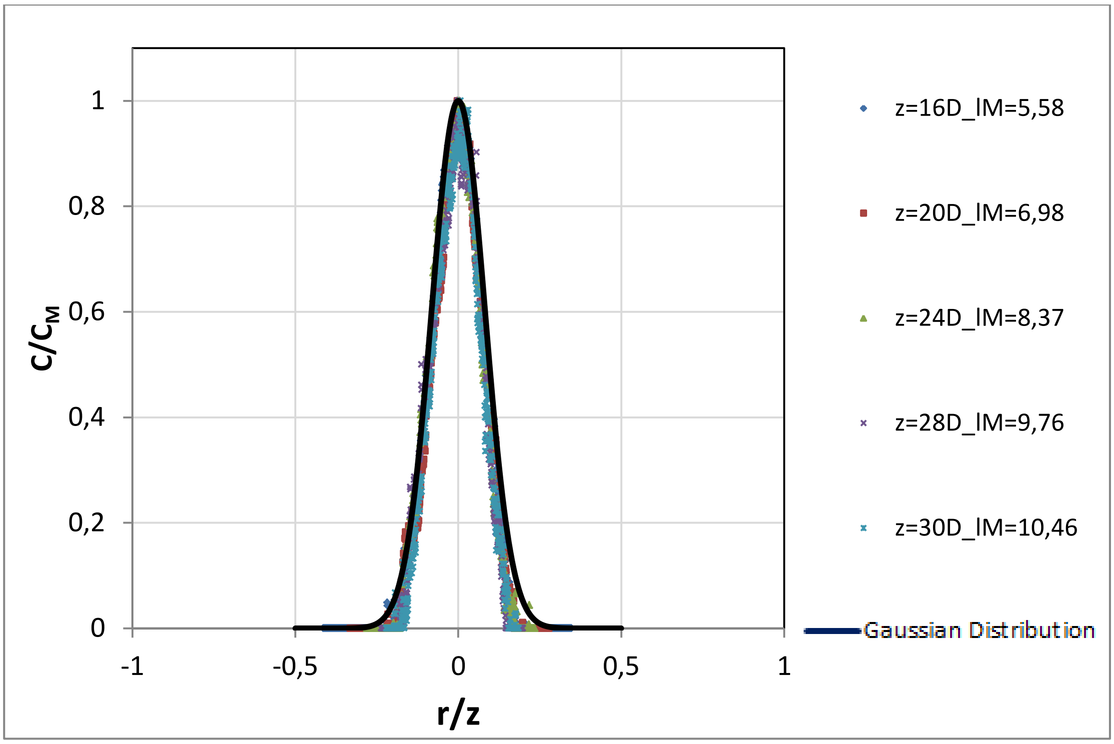

Figure A.21 Transverse distribution of the mean concentration at various vertical distances from the outflow from experiment Exp.11T

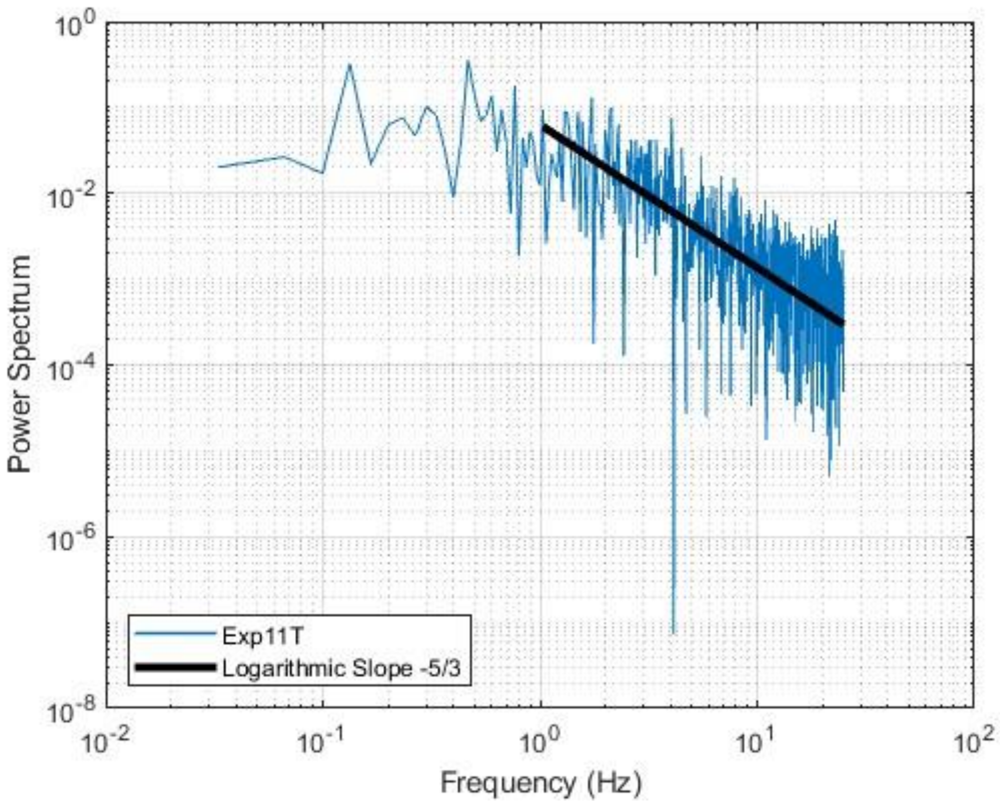

Figure A.22 Power spectral estimate at the buoyant jet centerline at dimensionless distance $z=5{,}84\ l_M$ for experiment Exp.11T